Key Selectivity Controlling Elements in Rhodium-Catalyzed C–H Functionalization with Donor/Acceptor Carbenes.

Zhi Ren,*,[1,2] Djamaladdin G. Musaev,*,[1,3] and Huw M. L. Davies*,[1]

[1]Department of Chemistry, Emory University, 1515 Dickey Drive, Atlanta, Georgia, United States 30322.

[2]College of Pharmacy, Shenzhen Technology University, 3002 Lantian Road, Shenzhen, Guangdong, China 518118.

[3]Cherry L. Emerson Center for Scientific Computation, Emory University, 1521 Dickey Drive, Atlanta, Georgia, 30322.

ABSTRACT: Computational studies on the dirhodium(tetracarboxylate)-catalyzed C—H functionalization with donor/acceptor carbenes reveal that the enantioselectivity and site-selectivity of this reaction are controlled by the ratio of conformers of both the diazo compound and the dirhodium carbene intermediates, and two distinct steps of the reaction, namely, nitrogen extrusion and carbene insertion in the functionalized C–H bond. In these studies, we used trichloroethyl phenyldiazoacetate as the carbene precursor, *p*-isopropyltoluene as the substrate, and dirhodium-tetraacetate and a chiral dirhodium complex, Rh_2(*S*-*p*-BrTPCP)$_4$, as the catalysts. While the aryldiazoacetate exists in two conformers, we found that the reaction is not under Curtin Hammett conditions because the barrier for nitrogen extrusion is less than the barrier for interconversion of aryldiazoacetate conformers. The resulting dirhodium carbene intermediates exist as a diastereomeric mixture, the ratio of which is governed by the ratio of the aryldiazoacetate conformers and the influence of the chiral catalyst on the nitrogen extrusion. The diastereomeric rhodium carbene complexes can, in principle, interconvert through rotation but the barrier for rotation is greater than the barrier for benzylic C—H functionalization. Thus, the two diastereomeric rhodium carbene complexes have different influences on the site- and enantio-selectivity of the reaction. In the particular case with the Rh_2(*S*-*p*-BrTPCP)$_4$-catalyzed reaction, the major rhodium carbene diastereomer is calculated to be the matched case, reacting in a highly enantioselective manner, whereas the minor rhodium carbene diastereomer gives low enantioselectivity. The overall predicted enantioselectivity of the reaction, 98.9:1.1 e. r., is in close agreement with its observed value of 97.5:2.5 e. r..

Catalyst-controlled selective C—H functionalization is a research area of intense current interest.[1] In the ideal system, simply choosing the right catalyst would control which C—H bond is functionalized and would overwhelm the natural reaction tendency of the substrate. Considerable advances have been made in recent years in the area of catalyst design[2] and enzyme evolution[3] to achieve systems capable of exquisite selectivity. One area where exceptional site selectivity has been achieved is the rhodium-catalyzed C(sp^3)—H functionalization by donor/acceptor carbenes.[2e,f] The generated catalytic active rhodium carbene intermediates during these reactions have the desirable properties of being sufficiently reactive to functionalize unactivated C—H bonds but are still greatly influenced by the steric environment of the catalyst, leading to selective reactions at primary, secondary or tertiary C—H bonds.

The mechanism for the rhodium-catalyzed C—H functionalization with diazoacetates is well established (see Scheme 1).[4] The first step of these reactions is accepted to be the nitrogen extrusion to form the carbene intermediate, which then undergoes the C—H functionalization in a concerted asynchronous manner. The asymmetric induction is considered to be dependent on which face of the rhodium-carbene complex is attacked. Even though the dirhodium catalysts have well defined structures,[2f,5] developing a clean mechanistic model to explain and predict the site selectivity and the enantioselectivity of these reactions has been challenging,[6] especially as some of the key steps have very small activation energies.[7] This has motivated us to re-examine some of the fundamental models and assumptions.

Scheme 1. Generally accepted mechanism for rhodium-catalyzed C—H functionalization with diazoacetates

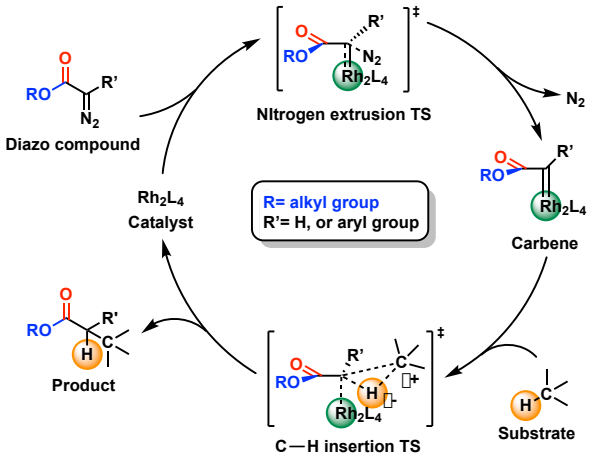

The seminal computational studies on the C—H functionalization chemistry of rhodium carbenes was conducted by Nakamura in 2002.[7a] That study began with an analysis of the dirhodium tetraformate-catalyzed reaction of diazomethane (**1**) and then extended to methyl diazoacetate (**2**) (Scheme 2). The nitrogen extrusion step to form the

rhodium-carbene was analyzed, followed by the C—H functionalization. An important observation from this study was the orientation of the ester orthogonal to the rhodium carbene plane, as shown in **3**. The C—H functionalization was considered to be a concerted asynchronous process with a hydridic transfer character (**TS-4**), as illustrated for the reaction with methyl diazoacetate with propane. The C—H functionalization was originally calculated to have a very low activation energy (0.2 kcal mol^{-1}),[7a] which illustrates the remarkable reactivity of these metal carbene intermediates. A more advanced calculation on the reaction with cyclopentane reported an activation energy of 3.5 kcal mol^{-1}.[7b] In 2009 we conducted computational studies on donor/acceptor carbenes and compared them with the acceptor carbene derived from methyl diazoacetate.[7b] These carbenes, as illustrated for **6** generated from methyl phenyldiazoacetate (**5**), are generally more stable and have higher activation barriers for C—H functionalization ranging from 17.4 kcal mol^{-1} for cyclopentane to 6.2 kcal mol^{-1} for the very reactive cyclohexadiene. These carbenes also have a distinctive structural feature with the acceptor group aligning orthogonal to the rhodium carbene plane, whereas the phenyl group remains in the same plane as the rhodium carbene (**6**). This characteristic has been confirmed by X-ray crystallographic structures of rhodium carbene intermediates.[8] Numerous other calculations have been reported on enantioselective rhodium-catalyzed reactions with donor/acceptor rhodium carbenes[6,9] and other carbenes,[10] many of which rely on the key concepts originally made in Nakamura' seminal studies.

Scheme 2. Schematic presentation of diazo compounds, carbene intermediates and C–H insertion transition states for the previously reported dirhodium complexes catalyzed C–H insertion reactions

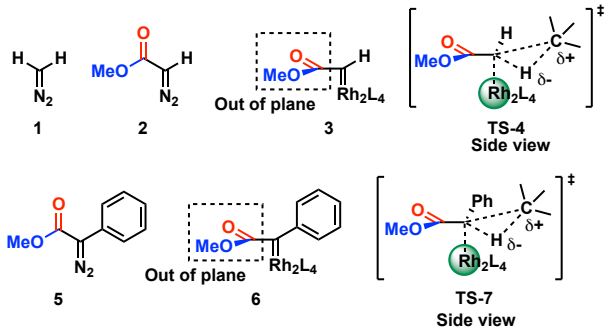

We have designed a number of chiral dirhodium catalysts for site selective and enantioselective C—H functionalization reactions of donor/acceptor carbenes.[2e,f] Our most recent chiral catalysts are sterically constrained and have been shown to adopt high symmetry chiral structures due to the specific arrangement of four identical carboxylate ligands around the dirhodium core.[2e,5] The 1,2,2-triarylcyclopropanecarboxylate (TPCP) ligands have been particularly effective and we have shown that they can adopt either C_2, C_4 or D_2 symmetric structures, which is dependent on the substitution pattern on the C1 aryl group.[2e,5] The earliest example of this type of catalyst is Rh$_2$(*S*-*p*-BrTPCP)$_4$ (**8**), which adopts a C_2-symmetric structure as illustrated in Figure 1.[5] One face of the rhodium is blocked and the other has an open groove for the carbene to bind and due to the C_2 symmetry, the two orientations of the carbene in the groove are identical (**Carbene A** and **B**).

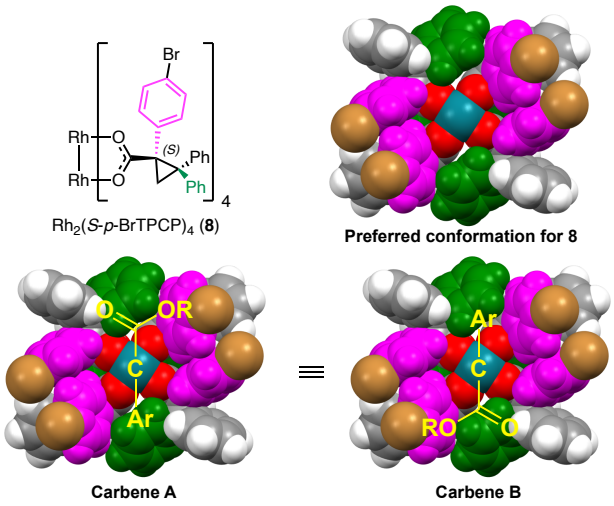

Figure 1. Preferred C_2 symmetry conformation of catalyst (**8**) and possible carbene coordination modes. The aryl ring with bromo substituent is colored in violet, and the phenyl group on C2 cis to carboxylate is colored in green. The carbene is colored in yellow. Due to the symmetry, carbene **A** and **B** are the same. The back face of the carbene is much more sterically crowded than the front face shown here.

A feature we recognized during these studies is that even though donor/acceptor carbenes are more stable than acceptor only carbenes, many of the reaction barriers are still very small.[6,7b] Consequently, factors that have not been considered in detail before, such as diazocarbonyl conformation or the ester orientation, may have a considerable influence on the outcome of the reaction. In order to understand the system more thoroughly, herein, we have selected to analysis of the C–H functionalization reaction of 2,2,2-trichloroethyl phenyldiazoacetate (**9**) and *p*-cymene (**10**) with dirhodium tetraacetate (**11**) as catalyst and then extended the findings to an analysis of the chiral dirhodium catalyst Rh$_2$(*S*-*p*-BrTPCP)$_4$ (**8**) (Figure 1). The trichloroethyl ester of the carbene was used because this ester group profoundly enhances site selective and diastereoselective C—H functionalization compared to the traditional methyl ester.[2f] This specific reaction was selected because it is one of the standard reactions used to evaluate the site selectivity profile of new dirhodium catalysts.[11] The dirhodium tetraacetate catalyzed reaction gives a preference for insertion into the tertiary C—H bond to form **12** (4:1 r.r.), whereas the Rh$_2$(*S*-*p*-BrTPCP)$_4$-catalyzed reaction strongly favors the primary C—H insertion product **13** (>20:1 r.r.). Furthermore, **13** is produced with high asymmetric induction (97.5:2.5 er, favoring the *R* isomer).[11b]

Scheme 3. Experimental results for *p*-cymene C—H functionalization by donor/acceptor carbene and dirhodium catalysts

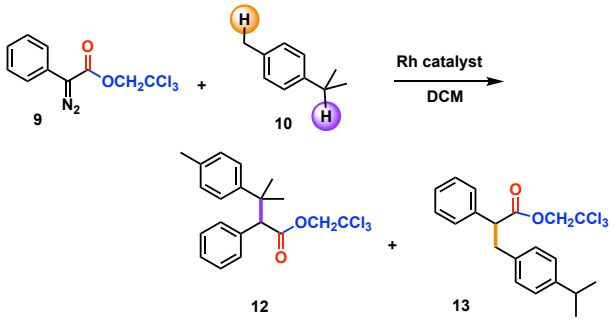

Catalyst	12:13	ee of 13
$Rh_2(OAc)_4$ (11)	83:17	—
Rh_2(*S*-*p*-BrTPCP)$_4$ (8)	<2:98	95% ee ((R)-13)

At first, we analyzed the nitrogen extrusion that leads to the dirhodium carbene intermediate (Scheme 1). While the previous studies established the nitrogen extrusion as the initial step, they did not explore the possibility that dinitrogen could leave from either side (i.e., alkoxy or carbonyl sides) of the ester group (**TS-14a** versus **TS-14b**) (Figure 2). It is irrelevant in the case of an achiral catalyst because the two transition states would form enantiomeric carbene intermediates **15** and **16**. Furthermore, the initial binding of the diazo compound could occur on either face of the dirhodium catalyst, which would switch which enantiomer of the carbene would be formed. However, this would not be the case for chiral catalysts with a defined binding site because **15** and **16** would now be diastereomers and if the interconversion between **15** and **16** was slower than the rate of the carbene reaction, then the mode of nitrogen extrusion could influence which rhodium carbene diastereomer contributes more to the overall reaction.

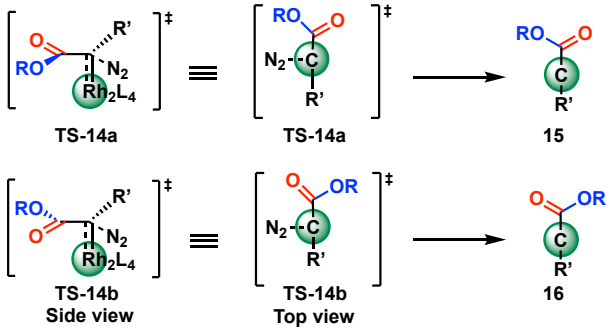

Figure 2. Analysis of nitrogen extrusion with an achiral catalyst. The alkoxy group of the ester is colored blue and the carbonyl group is colored red. In the top view, the green circle represents the dirhodium catalyst underneath the carbon atom. The two carbene structures, **15** and **16**, are shown in a top view.

The next step in the reaction is the carbene-induced C—H insertion as illustrated in Scheme 1. The preferred TS in the Nakamura's study was identified to be with the substrate approaching from the same face of the alkoxy group of the ester (Figure 3, blue arrow, via **TS-17a**).[7a] However, the possibility exists, especially in the case of chiral catalysts, that the established attack from the alkoxy side may not always be preferred and approach from the same side as the carbonyl (red arrow, via **TS-17b**) may occur. Indeed the subsequent computational analysis of donor/acceptor and other carbene reactions,[9,10] the majority have as the preferred transition state, the substrate approaching on the side of the alkoxy group, but approach on the carbonyl side has also been invoked in several cases.[9b, f, g, j, q, 10a, 2c-f] A systematic analysis of the two possible orientations of attack has not been reported. However, they may play an important role in the overall asymmetric induction of the process when chiral catalysts are used, because it would be possible to have either matched or miss-matched asymmetric induction during the carbene reaction. Therefore, we conduct a computational analysis to evaluate whether these stereochemical features have an influence on the overall outcome of the C–H functionalization.

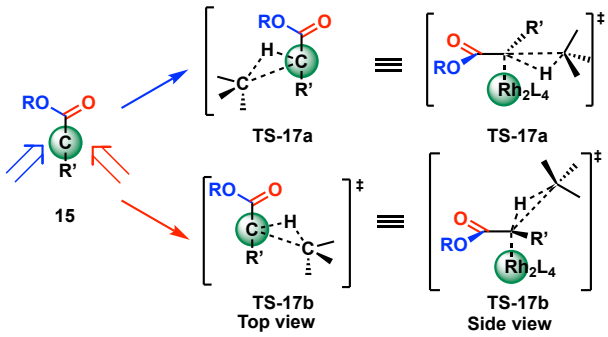

Figure 3. Analysis of the achiral catalyst $Rh_2(OAc)_4$ catalyzed carbene insertion into the C—H bond. The illustration is based on carbene **15**, which is shown aligned above the dirhodium. The alkoxy group of the ester is colored blue and the carbonyl group is colored red. In the top view, the green circle represents the dirhodium catalyst underneath the carbon atom.

To investigate the above proposed analyses, we used B3LYP density functional[12] augmented by the dispersion corrections (at the Grimme's empirical D3-level with the Becke-Johnson (BJ) damping)[13] as implemented in the Gaussian09 suite.[14] In these calculations, the 6-31G(d,p) and Lanl2dz basis sets were used for the main group atoms and Rh, respectively.[15,16] For Rh, we also used the Hay-Wadt effective core potential.[16] Frequency analysis was conducted to characterize each minimum and transition. Intrinsic reaction coordinate (IRC) calculations were performed for all TSs to ensure their true nature. Bulk solvent effects were incorporated at the conductor-like polarizable continuum model (C-PCM).[17] As a solvent we chose dichloromethane, which is the optimum solvent for these reactions. The calculated thermodynamic data are reported as ΔH/ΔG at the 298.15K temperature and 1 atm pressure. However, below, we only discuss the calculated Gibbs free energies, ΔG (see the Supporting Information for more details of the computation, as well as calculated energies and cartesian coordinates all reported structures).

At the onset of the study, we determined the preferred conformation of 2,2,2-trichloroethyl phenyldiazoacetate (**9**). The two conformers, **9a** and **9b**, and their interconversion barrier were computed, and the results are summarized in

Scheme 4. In these conformers, both the carbonyl and diazo groups are coplanar because they would stabilize the diazo functionality through conjugation. In **9a** the carbonyl group of the ester is s-*trans* to the diazo group, and in **9b** it is s-*cis* to the diazo group. The calculations revealed that the diazo compound prefers to adopt conformer **9a**, which is by 1.7 kcal mol^{-1} more favorable than conformer **9b** presumably to avoid dipole repulsion. Interconversion between these two conformers occurs by rotation of the ester group at the **TS-18** with a 13.0 kcal mol^{-1} free energy barrier.

Scheme 4. Schematic presentation of the two conformers, 9a and 9b, of diazo compound 9, and their interconversion transition state alongside with the calculated relative energies (in kcal mol^{-1})

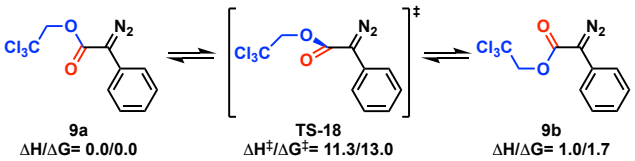

In the next stage, we examine how the two conformers of the aryldiazoacetate (**9a** and **9b**) would interact with the catalyst. The first round of calculations was conducted with dirhodium tetraacetate (**11**) as the catalyst (Scheme 5). There are three possible modes in which the diazo conformers could interact with this catalyst leading to the oxygen-coordinated complexes (**19a** and **19b**), nitrogen-coordinated complexes (**20a** and **20b**), and carbon-coordinated complexes (**21a** and **21b**). The difference between the **a** and **b** series is the conformation of the ester. The oxygen-coordinated complex **19a** is the thermodynamically most stable among the three groups of complexes and is set as the reference point for the discussion of energies of the calculated intermediates, transition states and products of the reaction. The complexes **19a**, **19b**, **20a**, **20b**, **21a**, and **21b** would most likely equilibrate by means of a dissociation-association pathway, because metal-migration by a concerted 1,3-shift is generally forbidden.[18]

Scheme 5. Possible isomeric forms of the complexes of diazo compound with $Rh_2(OAc)_4$ alongside with their relative energies (in kcal mol^{-1})

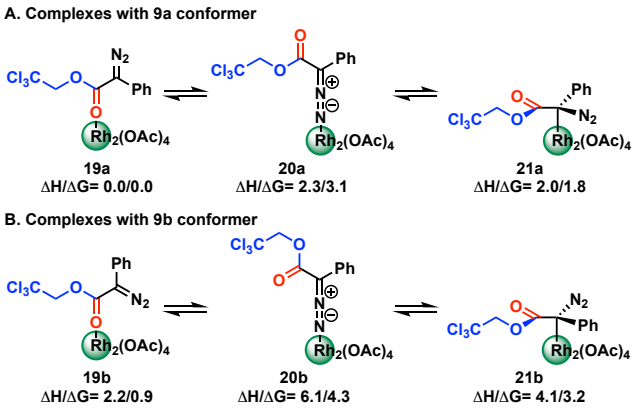

The detailed analysis of the intermediates involved in the nitrogen extrusion step is shown in Figure 4. Here, we consider formation of the rhodium carbene from both conformers of the diazo compound. The reaction from the s-*trans* conformer (**9a**) is highlighted in blue and the reaction from the s-*cis* conformer (**9b**) is highlighted in red. The rhodium carbenes **23** and **25** that would be formed from the two pathways are of the same energy because they are enantiomers. The two pathways to the rhodium carbenes are not equivalent since the dinitrogen is departing from either the carbonyl side or the alkoxy side of the ester group. The transition states for the two pathways (**TS-22a** and **TS-22b**) have relatively similar energy, which means that both pathways will be operational. Importantly, the nitrogen extrusion barriers of 11.4 and 10.1 kcal mol^{-1} at the transition states **TS-22a** and **TS-22b** (calculated relative to the pre-reaction carbon-coordinated complexes **21a** and **21b**) respectively, are lower than the associated **9a** → **9b** and reverse **9b** → **9a** interconversion barrier of 13.0 and 11.3 kcal mol^{-1}, respectively, reported above (see Scheme 4). This finding indicates that the Curtin-Hammett principle is not applicable for the nitrogen extrusion reaction, and the ratio of the diazo compounds **9a** and **9b** would determine the yield of the carbenes **23** and **25**. The nitrogen extrusion is strongly exothermic and would be expected to be irreversible.

The next step in the catalytic cycle would be the insertion of the carbene into the C—H bonds. Previous calculations have established the C—H functionalization barriers by the rhodium donor/acceptor carbenes has a range from 17.4 kcal mol^{-1} for an unactivated system such as cyclopentane to 6.2 kcal mol^{-1} for an activated system such as cyclohexadiene.[7] In order to elucidate whether the C—H bond insertion operates under Curtin-Hammett conditions,[19] we have calculated the interconversion barrier for the carbene intermediates **23** and **25**. We found that it occurs by 14.3 kcal mol^{-1} free energy barrier at the transition state **TS-24** (Scheme 6) that associates by rotation around the carbene ester bond. This relatively high energy barrier is presumably because having the electron withdrawing group in the same plane as the carbene would electronically destabilize the highly electron deficient carbene center. Thus, the Curtin-Hammett principle is also not applicable in the $Rh_2(OAc)_4$-catalyzed reaction of the carbenes with activated substrates in which the activation energy of that step is

Scheme 6. Schematic presentation of the $(AcO)_4Rh_2$–carbene complexes and their interconversion transition state alongside with the calculated relative energies (in kcal mol^{-1})

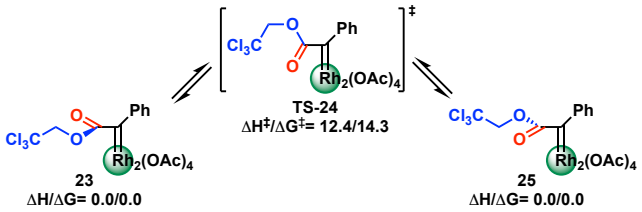

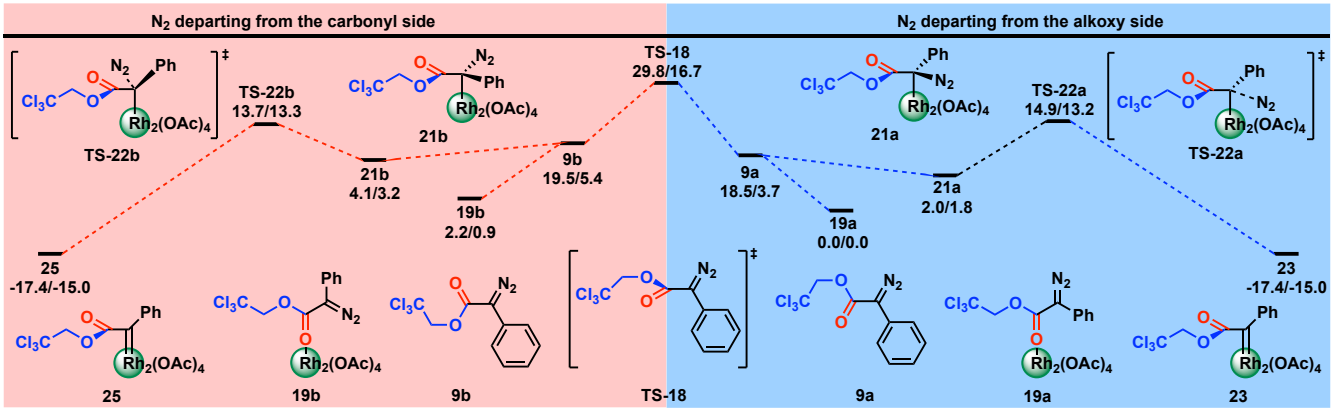

Figure 4. Free energy profiles of the nitrogen extrusion and dirhodium carbene formation upon the reaction of $Rh_2(OAc)_4$ with diazo conformers **9a** and **9b**. The scheme highlighted in blue is the reaction proceeding from the *s-trans* diazo compound **9a**. The scheme highlighted in red is the reaction proceeding from the s-*cis* diazo compound **9b**. Relative energies (in kcal/mol) are presented as ΔH/ΔG.

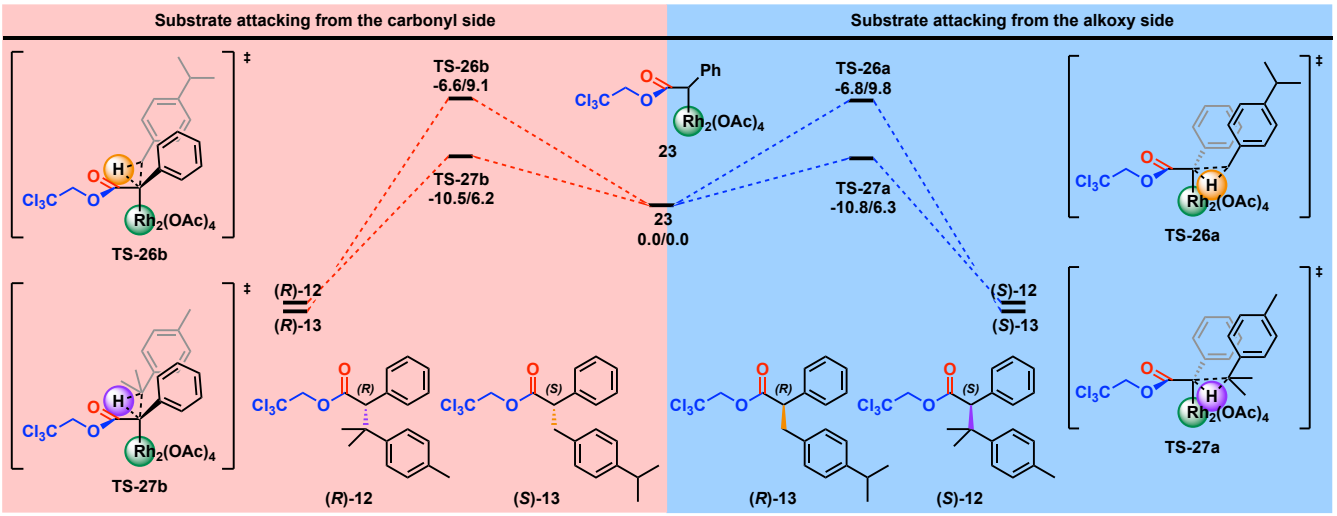

Figure 5. Free energy profiles of the C–H insertion in the carbene complex of $Rh_2(OAc)_4$. The scheme highlighted in blue is the reaction proceeding from attack at alkoxy side of the rhodium carbene **23**. The scheme highlighted in red is the reaction proceeding from attack at the carbonyl side of the rhodium carbene **23**. Both approaches predict that attack will preferentially occur at the tertiary benzylic site. Relative energies (in kcal/mol) are presented as ΔH/ΔG.

below about 14 kcal mol^{-1}. This would include C—H functionalization at activated sites,[7b] cyclopropanation,[7b] and cyclopropenation.[9d] In contrast, the $Rh_2(OAc)_4$-catalyzed carbene insertion into unactivated C—H bonds such as alkanes (which may require more than 14.3 kcal mol^{-1} free energy barrier) may operate under the Curtin-Hammett conditions.

In order to illustrate the controlling elements in a specific example, we have conducted a detailed analysis of the dirhodium tetraacetate-catalyzed reaction with *p*-cymene (**10**), which has site selectivity and enantioselectivity issues that need to be considered (Figure 5). For the sake of simplicity in our discussion, the rhodium carbene intermediates **23** and **25** were set as the reference points in the C—H insertion step. The free energy reaction profiles of the reactions illustrated in Figure 5 are based on the rhodium carbene **23.** The corresponding energy profile based on the rhodium carbene **25** would have the same energies providing the enantiomeric series of intermediates and products (see Supporting Information). The free energy difference between the transition states **TS-26a** (i.e., alkoxy side attack) and **TS-26b** (i.e., carbonyl side attack) would determine the facial selectivity of carbene **23**. Calculations established that the free energy barriers for the primary C—H insertion at **TS-26a** and **TS-26b** are 9.1 or 9.8 kcal mol^{-1}, respectively (which is smaller than the **23** ↔ **25** interconversion barrier of 14.3 kcal mol^{-1}). Thus, for primary C—H insertion in *p*-cymene, carbene **23** slightly prefers *re* face attack (the energy difference between the face-selectivity controlling transition states **TS-26a** and **TS-26b** is only 0.7 kcal mol^{-1}). In the meantime, carbene intermediate **25** would prefer the *si* face attack (see the Supporting Information) to the same extent as carbene **23**, leading to a racemate. As seen in Figure 5, the tertiary benzylic C—H bond functionalization transition states **TS-27a** and **TS-27b** have almost the same free energies. The regioselectivity of the

reaction is determined by the free energy difference of transition states **TS-26** and **TS-27** for the primary and tertiary benzylic C—H bond, respectively. The results indicate that the tertiary C—H insertion would be preferred over the primary C—H insertion when $Rh_2(OAc)_4$ used as the catalyst.

The overall view of the above presented study of the dirhodium tetraacetate-catalyzed primary C—H insertion is summarized in Figure 6. Since the *s-trans* (**9a**) and *s-cis* (**9b**) conformers of the diazo compound are not under equilibrium at the reaction condition (the calculated energy difference between them is 1.7 kcal mol^{-1}, and they are separated by 13.0 kcal mol^{-1} free energy barrier), the composition of the aryldiazoacetate is as 94% of **9a** and 6% of **9b**. As the catalyst is achiral, the enantiomeric pathways *via* **TS-22a** and **TS-22c** related to **9a** each contributed 47% of the formation of carbene **23** and **25**, and **TS-22b** and **TS-22d** related to **9b**, each contributed 3% to the formation of carbene **23** and **25**. Therefore, the ratio of carbene **23** and **25** would be 1:1, and 47% of each carbene is formed via dinitrogen departing from the alkoxy side, and 3% of each carbene is formed via dinitrogen departing from the carbonyl side. Carbene **23** is *re*-face selective to give 38% of **(*R*)-13** and 12% of **(*S*)-13**, while the enantiomeric carbene **25** is *si*-face selective and gives 38% of **(S)-13** and 12% of **(R)-13**. It needs to be emphasized that in the case of an achiral catalyst, the carbene would be equally able to bind to the other face of the dirhodium, leading to the opposite enantiomeric result.

The next stage of the study was to apply the concepts illustrated in Figure 6 to a chiral catalyst. Here, the benzylic C–H functionalization with the chiral catalyst Rh_2(*S-p*-BrTPCP)$_4$ (**8**) was used as the test reaction. As described in Figure 1, Rh_2(*S-p*-BrTPCP)$_4$ is a C_2 symmetric catalyst with a defined preferred binding site for the diazo compound on one face of the dirhodium complex. Even though there is a defined binding site for Rh_2(*S-p*-BrTPCP)$_4$, there will still be four possible nitrogen extrusion pathways leading to two diastereomeric rhodium carbene intermediates. For each carbene, the substrate can attack the carbene on the side of the alkoxy or the carbonyl group. The selectivity will be governed by the ratio of the two carbenes formed and how the two carbenes undergo the subsequent C—H functionalization. The concept of enantioselectivity being controlled by the combined effects of two discrete intermediates has been elegantly discussed by Blackmond[20] for the complex system where intermediates could equilibrate with each other and the staring materials. However, the system described herein is in some respect considerably simplified because: (a) both the nitrogen extrusion and C—H functionalization steps are considered irreversible, and (b) neither the starting material nor the intermediates equilibrate under the reaction conditions.

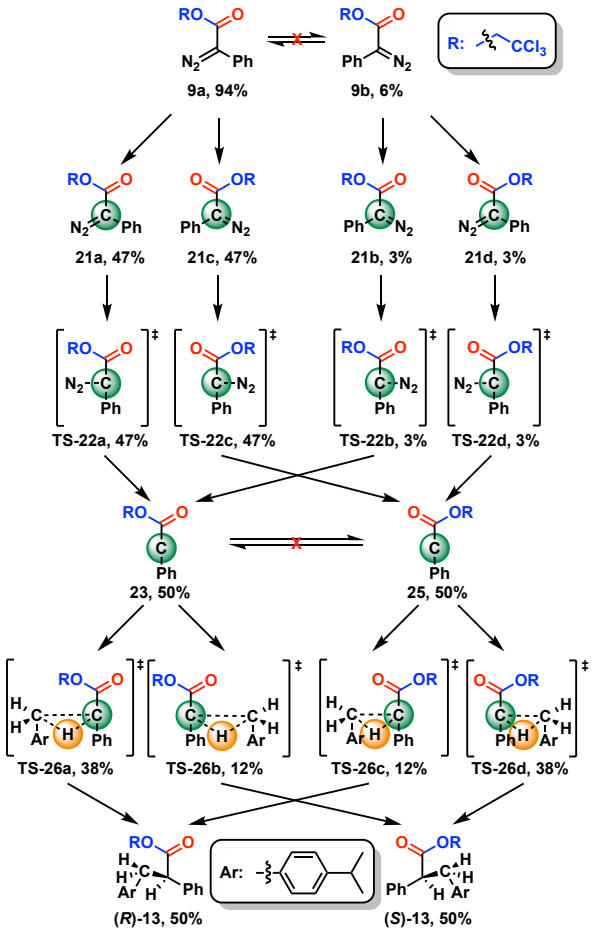

Figure 6. Summary of the proposed selectivity model for dirhodium catalyzed C—H insertion into activated C—H bonds.

We started our investigations focusing on the nitrogen extrusion step and optimized the four (**28a-d**) possible pre-reaction oxygen-coordinated and (**29a-d**) carbon-coordinated complexes (total of eight complexes, see Figure 7). The oxygen coordinated complexes **28a-d** are found to be more stable than the carbon coordinated complexes **29a-d**. The free energy of three of the oxygen bound complexes are within 1 kcal mol^{-1} of each other, leading to little reaction pathways preference, but the oxygen-coordinated complexes are not the on the pathway to the nitrogen extrusion and generation of the rhodium-carbenes. In contrast, a much greater preference was observed among the carbon-coordinated complexes **29a-d**, which are on the pathway to the nitrogen extrusion and generation of the rhodium-carbenes. The calculated structures **29a** and **29b** are the complexes with the *s-trans* aryldiazoacetate **9a**, and **29c** and **29d** are the complexes with the *s-cis* aryldiazoacetate **9b**. Nitrogen extrusion from **29a** and **29c** would generate the same diastereomer of the rhodium carbene, whereas **29b** and **29c** would generate the other diastereomer of the rhodium carbene. As seen in Figure 7, the carbon bound complex **29a** is by over 5 kcal mol^{-1} more stable than any of the other complexes **29b-d**. An examination of the model **29a** shows effective π-stacking between the aryl group of the carbene and two aryl groups of the ligands, an interaction absent in the other three structures **29b-d**.

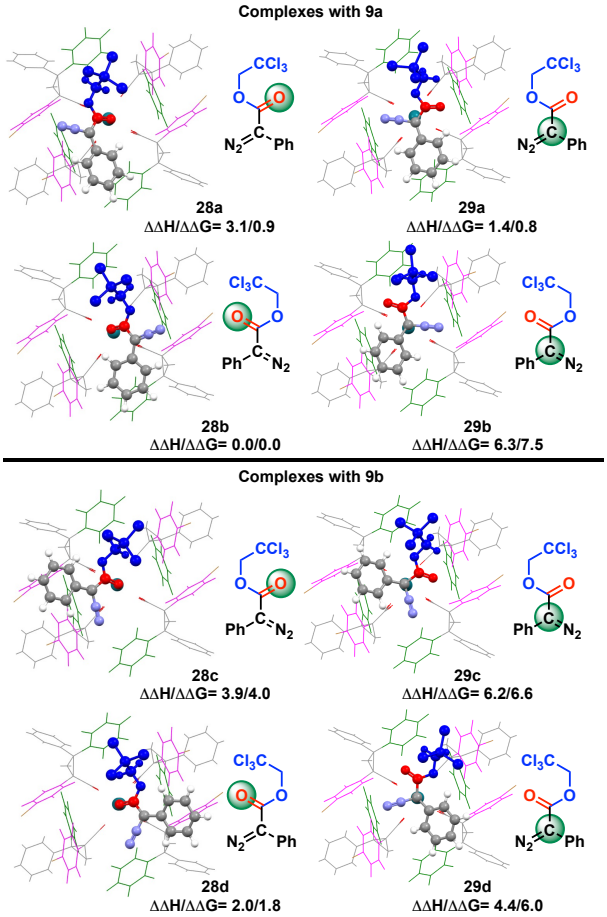

Figure 7. Schematic representation of the carbon-coordinated dirhodium–diazo complexes of the chiral catalyst Rh2(S-p-BrTPCP)4 (**8**), alongside with their calculated relative energies (in kcal mol-1). In the calculated structures, the ligands are shown in wireframe style, and the aryl ring with bromo substituent was colored in violet, and the phenyl group on C2 cis to carboxylate is colored green, and the diazo compound is in a ball and stick style, the carbonyl is colored red, and alkoxy group is colored blue.

Next, we computed the energy differences between the nitrogen extrusion TS structures (**TS-30a-d**) (Figure 8). In **TS-30a** and **TS-30b**, the nitrogen is departing from the alkoxy side of the ester group, while in the **TS-30c** and **TS-30d**, the nitrogen is departing from the carbonyl side of the ester group. As the rhodium complex is chiral, these TSs would be diastereomeric and their energies would be different. **TS-30a** and **TS-30b** are lowest in energy: thus, the nitrogen departing from the alkoxy side of the ester group is preferred. After the nitrogen departure, the carbene would be formed with the same orientation of ester group present in the TS structures. Therefore, **TS-30a** and **TS-30b** would generate one diastereomer of the rhodium carbene, and **TS-30c** and **TS-30d** would generate the other diastereomer.

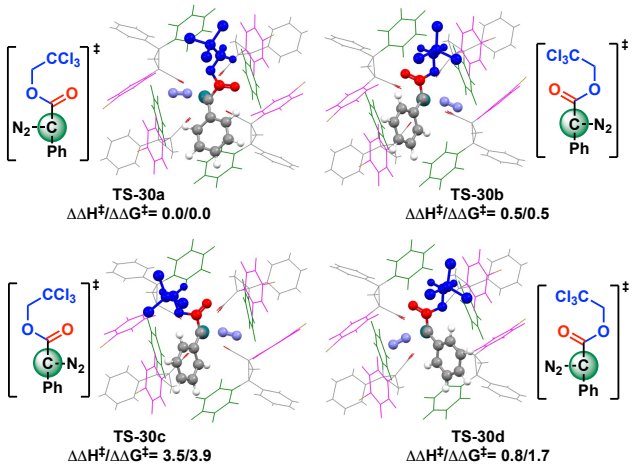

Figure 8. Illustration of detailed transition state (TS) structures for nitrogen extrusion in the chiral catalyst Rh2(S-p-BrTPCP)4 (8) catalyzed diazo compounds, alongside with their calculated relative energies (in kcal mol-1).

Carbenes (**31a** and **31b**) connected to these low-energy transition states are diastereomers, due to the chirality of the catalyst, and energy difference between them is 2.4 kcal mol^{-1} (**31a** is lowest one, see Figure 9). However, they are not in equilibrium, because the barrier for the subsequent C–H functionalization step is lower than the carbene interconversion barrier (See Supporting Information for details).

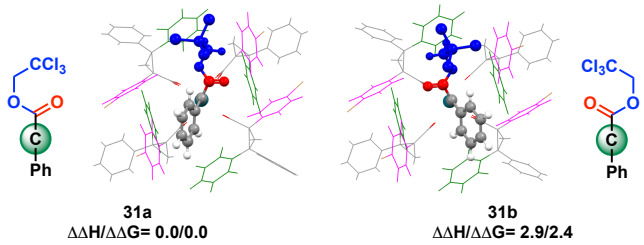

Figure 9. Illustration of detailed carbene structures in the chiral catalyst Rh$_2$(*S*-*p*-BrTPCP)$_4$ (**8**) catalyzed diazo compounds, alongside with their calculated relative energies (in kcal mol^{-1}).

The free energy profile for the key intermediates involved in the nitrogen extrusion with the chiral catalyst Rh$_2$(*S*-*p*-BrTPCP)$_4$ (**8**) are summarized in Figure 10. Once again, the reaction of both diazo conformers **9a** and **9b** are considered to be operating under non Curtin_Hammett conditions. A distinctive feature of the carbon-coordinated complexes **29** of Rh$_2$(*S*-*p*-BrTPCP)$_4$ (**8**) and aryldiazoacetate **9** is their high stability, relative to the dissociation limit of (**8**) + (**9**), compared to the corresponding intermediates of the reaction of **9** with dirhodium tetraacetate. As seen in Figure 10, the complexes **29a** and **29b,** driven from **9a**, are 19.2 and 12.5 kcal mol^{-1} stable relative to the dissociation limit of (**8**) + (**9a**). Similarly, the complexes **29c** and **29d,** driven from **9b**, are 16.7 and 17.3 kcal mol^{-1} stable relative to the dissociation limit of (**8**) + (**9b**). The larger stability of these rhodium-diazo complexes could be attributed to stronger diazo–ligand interaction, among other factors. Moreover, these complexation energies are even larger than the associated nitrogen extrusion barriers of 15.8, 9.6, 13.9, and

12.3 kcal mol^{-1} at the transition states **TS-30a**, **TS-30b**, **TS-30c**, and **TS-30d**, calculated relative to the corresponding carbon-coordinated complexes **29a**, **29b**, **29c**, and **29d**, respectively. Thus, for Rh$_2$(*S*-*p*-BrTPCP)$_4$ (**8**), (a) the carbon-coordinated diazo complexes **29a-d** are not under equilibrium during the reaction, and (b) *the nitrogen extrusion barriers calculated relative to these intermediates are smaller than the energy required for formation of free catalyst and free aryldiazoacetate from these intermediates.*

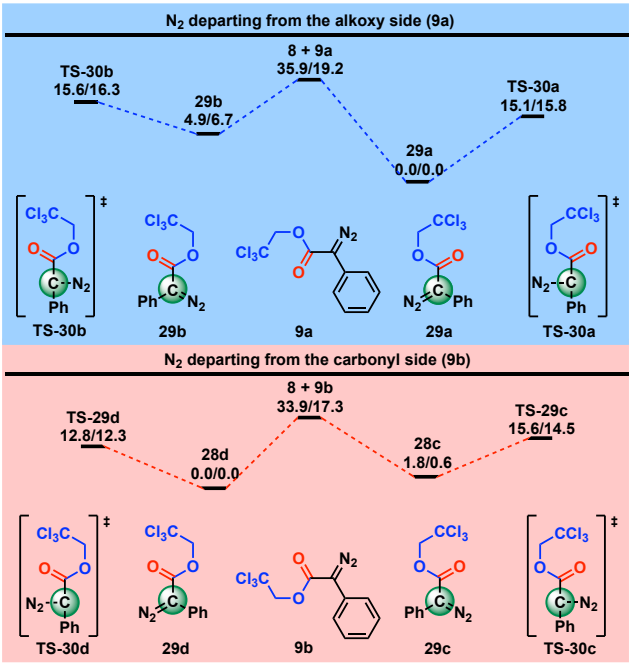

Figure 10. Free energy profiles of the C—H insertion in the carbon-coordinated diazo complexes of the chiral catalyst Rh$_2$(*S*-*p*-BrTPCP)$_4$ (**8**). The scheme highlighted in blue is the reaction proceeding from the *s-trans* diazo compound **9a**. The scheme highlighted in red is the reaction proceeding from the *s-cis* diazo compound **9b**. Relative energies (in kcal/mol) are presented as ΔH/ΔG.

The formation of carbene, **31a** and **31b**, via four **TS-30a-d** structures are summarized in Figure 11. The two conformers of diazo compounds are not interconverting under the reaction conditions, and neither are the dirhodium-diazo complexes. The composition ratio of the complexes **29a-d** determines the ratio of the generated carbene. Based on the above presented relative energies, (a) conformer **9a** is 94% of the total diazo compound composition, and (b) the associated carbon bound complex **29a** is by over 5 kcal mol^{-1} more stable than any of the other dirhodium-diazo complexes **29b-d**. Thus, the nitrogen extrusion by catalyst (**8**) from the major dirhodium-diazo conformer **29a** via **TS-30a** to give carbene **31a** is expected to be highly, with >99%, selective. But this is not the only pathway that carbene **31a** can be generated, because an additional amount could be generated from the minor diazo conformer, **9b**, via the complex **29c** and **TS-30c**. The face selectivity here is likely to be limited and if the activation energy runs parallel to the thermodynamic stability of the carbon-bound diazo compounds (the energy difference between the complexes **29c** and **29d**, generated from the minor diazo conformer **9b**, is calculated to be 0.6 kcal mol^{-1}, complex **29d** being as lowest in energy) one would predict that an 1.5% and 4.5% of carbenes **31a** and **31b**, respectively, would be generated from the minor diazo conformer, **9b.** Thus, the reaction of Rh$_2$(*S*-*p*-BrTPCP)$_4$ (**8**) to form the diastereomeric rhodium carbenes is highly selective with the major diazo conformer **9a** to form carbene **31a**, but the reaction with the minor conformer **9b** is far less selective, preferentially generating carbene **31b**. Also, the interconversion barrier for **31a** to **31b** was calculated to be 16.5 kcal mol^{-1}, which is higher than the following C—H insertion barriers with an activated substrate (See Supporting Information for details)

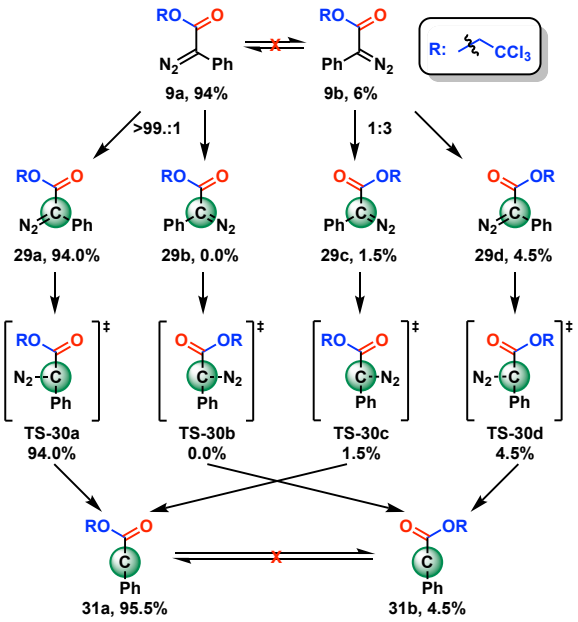

Figure 11. Illustration of the possible pathways to form carbene **31a** and **31b**.

Next, we investigate the C–H functionalization of *p*-cymene by the previously generated dirhodium-carbenes **31a** and **31b**. Here, we examined the transition states of the primary C–H functionalization reaction, because based on existing experiments[11b] he primary C–H insertion product is strongly preferred using the chiral catalyst Rh$_2$(*S*-*p*-BrTPCP)$_4$ (**8**). The facial selectivity for both carbenes were investigated by calculation of the TS with the substrate approaching from both side of the ester group. As seen in Figure 12, both carbene **31a** and **31b** prefer *re*-face attack, (**TS-32a** and **TS-32c**, respectively), which is consistent with the experimental observation. [11b] However, carbene **31a** is calculated to be highly enantioselective (>99.9:0.1 e.r., the calculated energy difference between the **TS-32a** and **TS-32b** is 5.0 kcal mol^{-1}), whereas carbene **31b** is calculated to be relatively unselective (3:1 e.r., the calculated ΔΔG$^{\#}$ [(**TS-32c)** – (**TS-32d)]** is 0.7 kcal mol^{-1}). As mentioned above (see Figure 11), the composition of **31a** and **31b** is 95.5% and 4.5%, respectively. Therefore, 95.5% carbene **31a** would give (*R*)-isomer as 95.5% of product **13**, and with an additional 3.4% of (*R*)-isomer of product **13** may came from **31b**. The (*S*)-isomer of product **13** is generated in 1.1% from carbene **31b** by means of **TS-32d**. The overall predicted enantiomeric ratio is 98.9:1.1 (98% ee), which is in excellent agreement with the experimental ratio of 97.5:2.5

(95% ee). To summarize, the enantioselectivity of the primary C–H bond functionalization by the donor/acceptor carbene and the chiral catalyst Rh_2(*S*-*p*-BrTPCP)$_4$ (**8**) is determined by several sequential factors: (a) the ratio of the diazo compound conformers, (b) the ratio of the dirhodium carbene intermediates, and (c) the facial selectivity of each carbene intermediate. *Thus, it is instructive that enhancement of enantioselectivity of the C–H functionalization could be achieved by improving the distribution ratio of both diazo compound and dirhodium carbene intermediate rather than just focusing on the likely carbene face selectivity.*

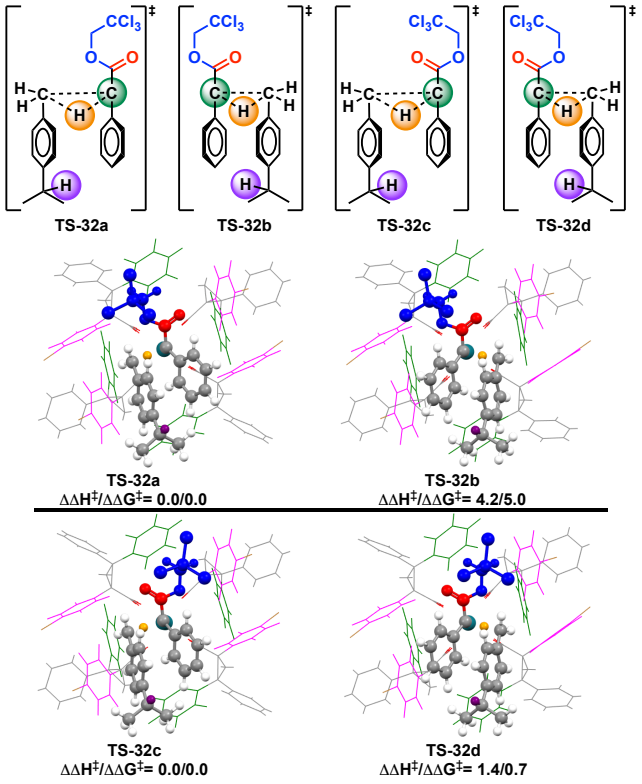

Figure 12. Illustration of detailed TS structures for primary benzylic C—H insertion step in the dirhodium–carbene complexes of the chiral catalyst Rh_2(*S*-*p*-BrTPCP)$_4$ (**8**), alongside with their calculated relative energies (in kcal mol^{-1}). The green circle represents the dirhodium catalyst underneath the carbon atom. The alkoxy group of the ester is colored blue and the carbonyl group is colored red. The transferring hydrogen atom of the primary C—H bond is highlighted by an orange circle, and the hydrogen atom at the tertiary C—H bond is highlighted by a purple circle. In the calculated structures, the ligands are shown in wireframe style, and the aryl ring with bromo substituent was colored in violet, and the phenyl group on C2 cis to carboxylate is colored green, and the carbene and substrate are in a ball and stick style, the transferring hydrogen atom is colored orange, and the tertiary benzylic hydrogen is colored purple.

As mentioned above and shown previously,[11b] Rh_2(*S*-*p*-BrTPCP)$_4$, strongly prefers formation of the primary C—H functionalization product. Here, we computationally investigated the regioselectivity of this reaction by comparing the free energy of TSs for the insertion of primary (**TS-32a**) and tertiary (**TS-33a**) benzylic C—H bonds (Figure 13). We found that transition state **TS-32a** is lower by 5.0 kcal mol^{-1} than the transition state **TS-33a**. This is in close agreement with the observed site selectivity, in which none of the tertiary C–H functionalization product was observed.[11b] Rh_2(*S*-*p*-BrTPCP)$_4$ is a sterically demanding catalyst and the change of site selectivity is considered to be due to steric factors overwhelming the electronic preference of the carbene C—H functionalization.

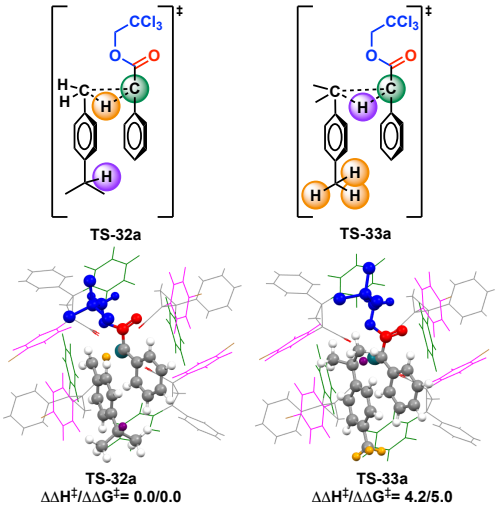

Figure 13. Comparison of TS structures of primary and tertiary benzylic C—H insertion in the dirhodium–carbene complexes of the chiral catalyst Rh_2(*S*-*p*-BrTPCP)$_4$ (**8**), alongside with their calculated relative energies (in kcal mol^{-1}). The green circle represents the dirhodium catalyst underneath the carbon atom. The alkoxy group of the ester was colored in blue and the carbonyl group was colored in red. The transferring hydrogen atom of the primary C—H bond was highlighted by orange circle, and the hydrogen atom at tertiary C—H bond was highlighted by purple circle. In the calculated structures, the ligands are shown in wireframe style, and the aryl ring with bromo substituent was colored in violet, and the phenyl group on C2 cis to carboxylate was colored in green, and the carbene and substrate were in ball and stick style, and the transferring hydrogen atom was colored in orange for the primary C—H bond, and colored in purple for the tertiary C—H bond.

In conclusion, the model presented herein indicates that the control of selectivity in dirhodium(tetracarboxylate)-catalyzed C–H bond functionalization by donor/acceptor diazo compounds is more complicated than previously suggested. It dependents on the ratio of conformers of the starting diazo compound and nature of two discrete steps, namely, the nitrogen extrusion and the carbene insertion steps. In most reactions, such as functionalization of activated C–H bonds (as well as the cyclopropanation, cyclopropenation, and ylide formation) the barriers the carbene insertion are sufficiently low that the reactions do not operate under Curtin Hammett conditions. We have shown that in the extensively utilized C–H bond functionalization by the donor/acceptor carbene and chiral catalyst Rh_2(S-p-BrTPCP)$_4$ (**8**), the enhancement of enantioselectivity of the C–H functionalization could be achieved by improving the distribution ratio of both diazo compound and dirhodium carbene intermediate rather than just focusing on the likely carbene face selectivity.

ASSOCIATED CONTENT

Supporting Information. Computational Methods and additional details about the computational results. This material is available free of charge via the Internet at http://pubs.acs.org.

AUTHOR INFORMATION

Corresponding Authors

*E-mail: hmdavie@emory.edu
*E-mail: dmusaev@emory.edu
*E-mail: renzhi@sztu.edu.cn

ACKNOWLEDGEMENT

This work was supported by the NSF under the Center for C–H Functionalization (CHE-1700982). We thank the members of the CCHF, especially Dr. Ken Houk and Dr. Donna Blackmond, for helpful discussions regarding this project. We appreciate Yannick T. Boni for conducting the experiments with both the achiral and chiral catalyst.

Conflict of Interest. HMLD is a named inventor on a patent entitled, Dirhodium Catalyst Compositions and Synthetic Processes Related Thereto (US 8,974,428, issued March 10, 2015). The other authors have no competing financial interests.

REFERENCES

(1) (a) Hartwig, J. F., Catalyst-Controlled Site-Selective Bond Activation. *Acc. Chem. Res.* **2017,** *50*, 549-555. (b) Hartwig, J. F.; Larsen, M. A., Undirected, Homogeneous C—H Bond Functionalization: Challenges and Opportunities. *ACS Cent. Sci.* **2016,** *2*, 281-292. (c) Gutekunst, W. R.; Baran, P. S., C–H functionalization logic in total synthesis. *Chem. Soc. Rev.* **2011,** *40*, 1976-1991. (d) Bruckl, T.; Baxter, R. D.; Ishihara, Y.; Baran, P. S., Innate and Guided C—H Functionalization Logic. *Acc. Chem. Res.* **2012,** *45*, 826-839. (e) Abrams, D. J.; Provencher, P. A.; Sorensen, E. J., Recent Applications of C—H Functionalization in Complex Natural Product Synthesis. *Chem. Soc. Rev.* **2018,** *47*, 8925-8967.

(2) (a) White, M. C.; Zhao, J., Aliphatic C—H Oxidations for Late-Stage Functionalization. *J. Am. Chem. Soc.* **2018,** *140*, 13988-14009. (b) Roizen, J. L.; Harvey, M. E.; Du Bois, J. Metal-Catalyzed Nitrogen-Atom Transfer Methods for the Oxidation of Aliphatic C-H Bonds. *Acc. Chem. Res.* **2012,** *45*, 911-922. (c) Doyle, M. P.; Liu, Y.; Ratnikov, M., Catalytic, Asymmetric, Intramolecular Carbon-Hydrogen Insertion. *Org. React. (Hoboken, NJ, U. S.)* **2013,** *80*, 1-131. (d) Doyle, M. P.; Duffy, R.; Ratnikov, M.; Zhou, L., Catalytic Carbene Insertion into C—H Bonds. *Chem. Rev.* **2010,** *110*, 704-724. (e) Davies, H. M. L.; Morton, D., Guiding Principles for Site Selective and Stereoselective Intermolecular C—H Functionalization by Donor/Acceptor Rhodium Carbenes. *Chem. Soc. Rev.* **2011,** *40*, 1857-1869. (f) Davies, H. M. L.; Liao, K. B., Dirhodium Tetracarboxylates as Catalysts for Selective Intermolecular C—H Functionalization. *Nat. Rev. Chem.* **2019,** *3*, 347-360. (g) Caballero, A.; Diaz-Requejo, M. M.; Fructos, M. R.; Olmos, A.; Urbano, J.; Perez, P. J., Catalytic Functionalization of Low Reactive C(sp^3)-H and C(sp^2)-H Bonds of Alkanes and Arenes by Carbene Transfer from Diazo Compounds. *Dalton Trans.* **2015,** *44*, 20295-20307. (h) Morton, C. M.; Zhu, Q. L.; Ripberger, H.; Troian-Gautier, L.; Toa, Z. S. D.; Knowles, R. R.; Alexanian, E. J., C—H Alkylation via Multisite-Proton-Coupled Electron Transfer of an Aliphatic C-H Bond. *J. Am. Chem. Soc.* **2019**, *141*, 13253-13260. (i) Quinn, R. K.; Konst, Z. A.; Michalak, S. E.; Schmidt, Y.; Szklarski, A. R.; Flores, A. R.; Nam, S.; Horne, D. A.; Vanderwal, C. D.; Alexanian, E. J., Site-Selective Aliphatic C—H Chlorination Using N-Chloroamides Enables a Synthesis of Chlorolissoclimide. *J. Am. Chem. Soc.* **2016**, *138*, 696-702.

(3) (a) Arnold, F. H., Innovation by Evolution: Bringing New Chemistry to Life (Nobel Lecture). *Angew. Chem. Int. Ed.* **2019**, *58*, 14420-14426. (b) Brandenberg, O. F.; Chen, K.; Arnold, F. H., Directed Evolution of a Cytochrome P450 Carbene Transferase for Selective Functionalization of Cyclic Compounds. *J. Am. Chem. Soc.* **2019,** *141*, 8989-8995. (c) Chen, K.; Zhang, S. Q.; Brandenberg, O. F.; Hong, X.; Arnold, F. H., Alternate Heme Ligation Steers Activity and Selectivity in Engineered Cytochrome P450-Catalyzed Carbene-Transfer Reactions. *J. Am. Chem. Soc.* **2018,** *140*, 16402-16407.

(4) (a) Davies, H. M. L.; Pelphrey, P. M. Intermolecular C—H Insertions of Carbenoids. *Org. React.* **2011**, *75*, 75-211. (a) Doyle, M. P.; Liu, Y.; Ratnikov, M., Catalytic, asymmetric, intramolecular carbon-hydrogen insertion. *Org. React.* **2013,** *80*, 1-131.

(5) Zhi, R.; Musaev, D. G.; Davies, H. M. L., Influence of Aryl Substituents on the Alignment of Ligands in the Dirhodium Tetrakis(1,2,2-Triarylcyclopropanecarboxylate) Catalysts, *ChemCatChem,* Early Access: September 2020, DOI: 10.1002/cctc.202001206.

(6) (a) Qin, C. M.; Boyarskikh, V.; Hansen, J. H.; Hardcastle, K. I.; Musaev, D. G.; Davies, H. M. L. D_2-Symmetric Dirhodium Catalyst Derived from a 1,2,2-Triarylcyclopropanecarboxylate Ligand: Design, Synthesis and Application. *J. Am. Chem. Soc.* **2011,** *133*, 19198-19204. (b) Liao, K. B.; Negretti, S.; Musaev, D. G.; Bacsa, J.; Davies, H. M. L. Site-Selective and Stereoselective Functionalization of Unactivated C-H Bonds. *Nature* **2016**, *533*, 230-234. (c) Liao, K. B.; Yang, Y. F.; Lie, Y. Z.; Sanders, J. N.; Houk, K. N.; Musaev, D. G.; Davies, H. M. L. Design of Catalysts for Site-Selective and Enantioselective Functionalization of Non-Activated Primary C-H Bonds. *Nature Chem.* **2018**, *10*, 1048-1055. (d) Liao, K.; Pickel, T. C.; Boyarskikh, V.; Bacsa, J.; Musaev, D. G.; Davies, H. M. L., Site-Selective and Stereoselective Functionalization of Non-activated Tertiary C-H Bonds. *Nature* **2017,** *551*, 609-613.

(7) (a) Nakamura, E.; Yoshikai, N.; Yamanaka, M., Mechanism of C-H Bond Activation/C-C Bond Formation Reaction between Diazo Compound and Alkane Catalyzed by Dirhodium Tetracarboxylate. *J. Am. Chem. Soc*. **2002**, *124*, 7181-7192. (b) Hansen, J.; Autschbach, J.; Davies, H. M. L. Computational Study on the Selectivity of Donor/Acceptor-Substituted Rhodium Carbenoids. *J. Org. Chem.* **2009,** *74*, 6555-6563.

(8) (a) Werle, C.; Goddard, R.; Philipps, P.; Fares, C.; Furstner, A., Stabilization of a Chiral Dirhodium Carbene by Encapsulation and a Discussion of the Stereochemical Implications. *Angew. Chem. Int. Ed.* **2016**, *55*, 10760-10765. (b)Werle, C.; Goddard, R.; Philipps, P.; Fares, C.; Furstner, A., Structures of Reactive Donor/Acceptor and Donor/Donor Rhodium Carbenes in the Solid State and Their Implications for Catalysis. *J. Am. Chem. Soc.* **2016**, *138*, 3797-3805.

(9) (a) Nowlan, D. T.; Gregg, T. M.; Davies, H. M. L.; Singleton, D. A. Isotope Effects and the Nature of Selectivity in Rhodium-Catalyzed Cyclopropanations. *J. Am. Chem. Soc.* **2003,** *125*, 15902-15911. (b) DeAngelis, A.; Dmitrenko, O.; Yap, G. P. A.; Fox, J. M. Chiral Crown Conformation of Rh_2(*S*-PTTL)$_4$: Enantioselective Cyclopropanation with α-Alkyl-α-diazoesters. *J. Am. Chem. Soc.* **2009,** *131*, 7230-7231. (c) Hansen, J.; Li, B.; Dikarev, E.; Autschbach, J.; Davies, H. M. L. Combined Experimental and Computational Studies of Heterobimetallic Bi-Rh Paddlewheel Carboxylates as Catalysts for Metal Carbenoid Transformations. *J. Org. Chem.* **2009,** *74*, 6564-6571. (d) Briones, J. F.; Hansen, J.; Hardcastle, K. I.; Autschbach, J.; Davies, H. M. L. Highly Enantioselective Rh_2(*S*-DOSP)$_4$-Catalyzed Cyclopropenation of Akynes with Styryldiazoacetates. *J. Am. Chem. Soc.* **2010,** *132*, 17211-17215. (e) Hansen, J. H.; Gregg, T. M.; Ovalles, S. R.; Lian, Y. J.; Autschbach, J.; Davies, H. M. L. On the Mechanism and Selectivity of the Combined C-H Activation/Cope Rearrangement. *J. Am. Chem. Soc.* **2011,** *133*, 5076-5085. (f) DeAngelis, A.; Dmitrenko, O.; Fox, J. M. Rh-Catalyzed intermolecular Reactions of Cyclic alpha-Diazocarbonyl Compounds with Selectivity over Tertiary C-H Bond Migration. *J. Am. Chem. Soc.* **2012,** *134*, 11035-11043. (g) Wang, H. B.; Guptill, D. M.; Varela-Alvarez, A.; Musaev, D. G.; Davies, H. M. L. Rhodium-Catalyzed Enantioselective

Cyclopropanation of Electron-Deficient Alkenes. *Chem. Sci.* **2013,** *4*, 2844-2850. (h) Kisan, H. K.; Sunoj, R. B. Axial Coordination Dichotomy in Dirhodium Carbenoid Catalysis: A Curious Case of Cooperative Asymmetric Dual-Catalytic Approach Toward Amino Esters. *J. Org. Chem.* **2015,** *80*, 2192-2197. (i) Xie, Q.; Song, X. S.; Qu, D.; Guo, L. P.; Xie, Z. Z. DFT Study on the Rhodium(II)-Catalyzed C-H Functionalization of Indoles: Enol Versus Oxocarbenium Ylide. *Organometallics* **2015,** *34*, 3112-3119. (j) Liu, H.; Duan, J. X.; Qu, D. Y.; Guo, L. P.; Xie, Z. Z. Mechanistic Insights into Asymmetric C-H Insertion Cooperatively Catalyzed by a Dirhodium(II) Complex and Chiral Phosphoric Acid. *Organometallics* **2016,** *35*, 2003-2009. (k) Liu, Y.; Luo, Z. J.; Zhang, J. Z.; Xia, F. DFT Calculations on the Mechanism of Transition-Metal-Catalyzed Reaction of Diazo Compounds with Phenols: O-H Insertion Versus C-H Insertion. *J. Phys. Chem. A* **2016,** *120*, 6485-6492. (l) Yang, X.; Yang, Y. S.; Rees, R. J.; Yang, Q.; Tian, Z. Y.; Xue, Y. How Dirhodium Catalyst Controls the Enantioselectivity of 3+2 -Cycloaddition Between Nitrone and Vinyldiazoacetate: A Density Functional theory study. *J. Org. Chem.* **2016,** *81*, 8082-8086. (m) Liu, S. Y.; Jiang, J.; Chen, J. H.; Wei, Q. H.; Yao, W. F.; Xia, F.; Hu, W. H. A DFT Calculation-Inspired Rh(I)-Catalyzed Reaction via Suppression of alpha-H Shift in alpha-Alkyldiazoacetates. *Chem. Sci.* **2017,** *8*, 4312-4317. (n) Fu, J. T.; Ren, Z.; Bacsa, J.; Musaev, D. G.; Davies, H. M. L. Desymmetrization of Cyclohexanes by Site- and Stereoselective C-H Functionalization. *Nature* **2018,** *564*, 395. (o) Zhou, M. J.; Springborg, M. Theoretical Study of the Mechanism Behind the Site- and Enantioselectivity of C-H Functionalization Catalysed by Chiral Dirhodium Catalyst. *Phys. Chem. Chem. Physi.* **2020,** *22*, 9561-9572. (p) Wen, M.; Li, S.; Han, J.; Xue, Y. Mechanism and Enantioselectivity of the Asymmetric [3+2]-Annulation Between N-Methylindole and Enoldiazoacetamide Catalyzed by Prolinate-Coordinated Dirhodium: A theoretical study. *J. Mol. Graphics Modell.* **2020,** *94*, 107489.

(10) (a) Yoshikai, N.; Nakamura, E. Theoretical Studies on Diastereo- and Enantioselective Rhodium-Catalyzed Cyclization of Diazo Compound via Intramolecular C-H Bond Insertion. *Adv. Synth. Catal.* **2003,** *345*, 1159-1171. (b) Howell, J. A. S. On the Mechanism of the Rh(II)-Catalysed Cyclopropanation of Alkenes. *Dalton Trans.* **2007,** 1104-1114. (c) Bonge, H. T.; Hansen, T. Computational comparison of $Rh_2(esp)_2$ and $Rh_2(O_2CH)_4$ as Catalysts in a Carbenoid Reaction. *Tetrahedron Lett.* **2010,** *51*, 5298-5301. (d) Bonge, H. T.; Hansen, T. Computational Study of C-H Insertion Reactions with Ethyl Bromodiazoacetate. *Eur. J. Org. Chem.* **2010,** 4355-4359. (e) Bonge, H. T.; Hansen, T. Computational Study of Cyclopropanation Reactions with Halodiazoacetates. *J. Org. Chem.* **2010,** *75*, 2309-2320. (f) Bonge, H. T.; Hansen, T. Insights on Rh(II) Carbenoid Reactivity. *Tetrahedron Lett.* **2010,** *51*, 5378-5381. (g) Boultadakis-Arapinis, M.; Gandon, V.; Prost, E.; Micouin, L.; Lecourt, T. Electronic Effects in Carbene-Mediated C-H Bond Functionalization: An Experimental and Theoretical Study. *Adv. Synth. Catal.* **2014,** *356*, 2493-2505. (h) Xue, Y. S.; Cai, Y. P.; Chen, Z. X. Mechanism and Stereoselectivity of the Rh(II)-Catalyzed Cyclopropanation of Diazooxindole: A Density Functional Theory Study. *RSC Advances* **2015,** *5*, 57781-57791. (i) Mai, B. K.; Szabo, K. J.; Himo, F. Mechanisms of Rh-Catalyzed Oxyaminofluorination and Oxyaminotrifluoromethylthiolation of Diazocarbonyl Compounds with Electrophilic Reagents. *Org. Lett.* **2018,** *20*, 6646-6649. (j) McLarney, B. D.; Hanna, S.; Musaev, D. G.; France, S. Predictive Model for the $Rh_2(esp)_2$-Catalyzed Intermolecular C(sp^3)-H bond Insertion of beta-Carbonyl Ester Carbenes: Interplay Between Theory and Experiment. *ACS Catalysis* **2019,** *9*, 4526-4538. (k) General review: Sperger, T.; Sanhueza, I. A.; Kalvet, I.; Schoenebeck, F. Computational Studies of Synthetically Relevant Homogeneous Organometallic Catalysis Involving Ni, Pd, Ir, and Rh: An Overview of Commonly Employed DFT Methods and Mechanistic Insights. *Chem. Rev.* **2015,** *115*, 9532-9586.

(11) (a) Guptill, D. M.; Davies, H. M. L. 2,2,2-Trichloroethyl Aryldiazoacetates as Robust Reagents for the Enantioselective C-H Functionalization of Methyl Ethers. *J. Am. Chem. Soc.* **2014,** *136*, 17718-17721. (b) Qin, C. M.; Davies, H. M. L. Role of Sterically Demanding Chiral Dirhodium Catalysts in Site-Selective C-H Functionalization of Activated Primary C-H Bonds. *J. Am. Chem. Soc.* **2014,** *136*, 9792-9796.

(12) (a) Becke, A. D. Density-Functional Exchange-Energy Approximation with Correct Asymptotic Behavior. *Phys. Rev. A* **1988,** *38*, 3098-3100. (b) Lee, C.; Yang, W.; Parr, R. G. Development of The Colle-Salvetti Correlation-Energy Formula into a Functional of the Electron Density. *Phys. Rev. B* **1988,** *37*, 785-789. (c) Becke, A. D. A New Mixing of Hartree – Fock and Local Density - Functional Theories. *J. Chem. Phys.* **1993,** *98*, 1372-1377.

(13) (a) Grimme, S.; Antony, J.; Ehrlich, S.; Krieg, H. A Consistent and Accurate Ab Initio Parametrization of Density Functional Dispersion Correction (DFT-D) for the 94 Elements H-Pu. *J. Chem. Phys.* **2010,** *132*, 154104-154122. (b) Becke, A. D.; Johnson, E. R. A Density-Functional Model of the Dispersion Interaction. *J. Chem. Phys.* **2005,** *123*, 154101-154106. (c) Becke, A. D.; Johnson, E. R. Exchange-Hole Dipole Moment and the Dispersion Interaction. *J. Chem. Phys.* **2005,** *122*, 154104-154109. (d) Johnson, E. R.; Becke, A. D. A Post-Hartree-Fock Model of Intermolecular Interactions: Inclusion of Higher-Order Corrections. *J. Chem. Phys.* **2006,** *124*, 174104-174112.

(14) Gaussian 09, Revision E.01, Frisch, M. J.; Trucks, G. W.; Schlegel, H. B.; Scuseria, G. E.; Robb, M. A.; Cheeseman, J. R.; Scalmani, G.; Barone, V.; Mennucci, B.; Petersson, G. A.; Nakatsuji, H.; Caricato, M.; Li, X.; Hratchian, H. P.; Izmaylov, A. F.; Bloino, J.; Zheng, G.; Sonnenberg, J. L.; Hada, M.; Ehara, M.; Toyota, K.; Fukuda, R.; Hasegawa, J.; Ishida, M.; Nakajima, T.; Honda, Y.; Kitao, O.; Nakai, H.; Vreven, T.; Montgomery, J. A., Jr.; Peralta, J. E.; Ogliaro, F.; Bearpark, M.; Heyd, J. J.; Brothers, E.; Kudin, K. N.; Staroverov, V. N.; Kobayashi, R.; Normand, J.; Raghavachari, K.; Rendell, A.; Burant, J. C.; Iyengar, S. S.; Tomasi, J.; Cossi, M.; Rega, N.; Millam, M. J.; Klene, M.; Knox, J. E.; Cross, J. B.; Bakken, V.; Adamo, C.; Jaramillo, J.; Gomperts, R.; Stratmann, R. E.; Yazyev, O.; Austin, A. J.; Cammi, R.; Pomelli, C.; Ochterski, J. W.; Martin, R. L.; Morokuma, K.; Zakrzewski, V. G.; Voth, G. A.; Salvador, P.; Dannenberg, J. J.; Dapprich, S.; Daniels, A. D.; Farkas, Ö.; Foresman, J. B.; Ortiz, J. V.; Cioslowski, J.; Fox, D. J. Gaussian, Inc., Wallingford CT, 2009

(15) Rassolov, V. A.; Pople, J. A.; Ratner, M. A.; Windus, T. L. 6-31G* basis set for atoms K through Zn. *J. Chem. Phys.* 1998, *109*, 1223-1229.

(16) (a) Hay, P. J.; Wadt, W. R. Ab Initio Effective Core Potentials for Molecular Calculations. Potentials for the Transition Metal Atoms Sc to Hg. *J. Chem. Phys.* **1985**, *82*, 270-283. (b) Hay, P. J.; Wadt, W. R. Ab Initio Effective Core Potentials for Molecular Calculations. Potentials for K to Au Including the Outermost Core Orbitals. *J. Chem. Phys.* **1985**, *82*, 299-310. (c) Wadt, W. R.; Hay, P. J. Ab Initio Effective Core Potentials for Molecular Calculations. Potentials for Main Group Elements Na to Bi. *J. Chem. Phys*. **1985**, *82*, 284-298.

(17) (a) Barone, V.; Cossi, M. Quantum Calculation of Molecular Energies and Energy Gradients in Solution by a Conductor Solvent Model. *J. Phys. Chem. A* **1998**, *102*, 1995-2001. (b) Cossi, M.; Rega, N.; Scalmani, G.; Barone, V. Energies, Structures, and Electronic Properties of Molecules in Solution with the C-PCM Solvation Model. *J. Comput. Chem.* **2003**, *24*, 669-681.

(18) Seeman, J. I. Effect of Conformational Change on Reactivity in Organic Chemistry: Evaluations, Applications, and Extensions of Curtin–Hammett and Winstein–Holness Kinetics, *Chem. Rev.* **1983**, *83*, 83–134.

(19) Woodward, R.B.; Hoffmann, R. The Conservation of Orbital Symmetry. Verlag Chemie Academic Press. 2004.

(20) Bures, J.; Armstrong, A.; Blackmond, D. G. Explaining Anomalies in Enamine Catalysis: "Downstream Species" as a New Paradigm for Stereocontrol. *Acc. Chem. Res.* **2016**, *49*, 214–222.

SYNOPSIS TOC